Luo *et al. Virology Journal* (2024) 21:217
https://doi.org/10.1186/s12985-024-02472-1

Virology Journal

RESEARCH

Open Access

The protective role of Mertk in JEV-induced encephalitis by maintaining the integrity of blood–brain barrier

Chuanyu Luo[1†], Mengyuan Li[2†], Peiyu Bian[3], Jiali Yang[4], Xiamei Liao[5], Yangchao Dong[5], Chuantao Ye[2], Fanglin Zhang[5], Xin Lv[5*], Qianqian Zhang[6*] and Yingfeng Lei[5*]

Abstract

Japanese encephalitis is an acute infectious disease of the central nervous system caused by neurotropic Japanese encephalitis virus (JEV). As a member of TAM (Tyro3, Axl and Mertk) family, Mertk has involved in multiple biological processes by engaging with its bridging ligands Gas6 and Protein S, including invasion of pathogens, phagocytosis of apoptotic cells, inflammatory response regulation, and the maintenance of blood brain barrier (BBB) integrity. However, its role in encephalitis caused by JEV infection has not been studied in detail. Here, we found that Mertk$^{-/-}$ mice exhibited higher mortality and more rapid disease progression than wild-type mice after JEV challenge. There were no significant differences in viral load and cytokines expression level in peripheral tissues between Wild type and Mertk$^{-/-}$ mice. Furthermore, the absence of Mertk had little effect on the inflammatory response and immunopathological damage while it can cause an increased viral load in the brain. For the in vitro model of BBB, Mertk was shown to maintain the integrity of the BBB. In vivo, Mertk$^{-/-}$ mice exhibited higher BBB permeability and lower BBB integrity. Taken together, our findings demonstrate that Mertk acts as a protective factor in the development of encephalitis induced by JEV infection, which is mainly associated with its beneficial effect on BBB integrity, rather than its regulation of inflammatory response.

Keywords Mertk, Japanese encephalitis virus, TAM receptors, Blood–brain barrier, Encephalitis

†Chuanyu Luo and Mengyuan Li have contributed equally for this work.

*Correspondence:
Xin Lv
luxin@fmmu.edu.cn
Qianqian Zhang
zhangqianyd@163.com
Yingfeng Lei
yflei@fmmu.edu.cn
[1] Department of Clinical Laboratory, Norinco General Hospital, Xi'an 710065, China
[2] Department of Infectious Diseases, Tangdu Hospital, Air Force Medical University, Xi'an 710032, China
[3] Department of Geriatrics, Xijing Hospital, Air Force Medical University, Xi'an 710032, China
[4] Department of Cell Biology, National Translational Science Center for Molecular Medicine, Air Force Medical University, Xi'an 710032, China
[5] Department of Microbiology and Pathogen Biology, School of Basic Medical Sciences, Air Force Medical University, Changle West Road, Xincheng District, Xi'an 710032, Shaanxi, China
[6] Department of Microbiology, Medical College, Yan'an University, Yan'an 716000, China

Introduction

Japanese encephalitis virus (JEV) is a mosquito-borne zoonotic flavivirus, which is the main cause of viral encephalitis in Asian countries but with no specific treatment available. JEV is a single-stranded positive-sense RNA virus belonging to the genus Flavivirus, which is mainly transmitted by animal vectors such as Culex tritaeniorhynchus, birds, bats and snakes [1–3]. JEV is a highly neurotropic flavivirus that can break through host bloodbrain barrier (BBB), causing neuronal infection, microglia activation, and eventually fatal Japanese encephalitis (JE) [4]. JEV is widely prevalent in Asian region with an estimated 68,000 clinical cases annually. Although symptomatic JE after JEV infection is relatively rare, the rate of fatal case among JE patients can reach 30%. Nearly half of the patients suffer from permanent neurological and psychiatric sequelae. Despite the safe and effective JEV vaccine has greatly reduced the incidence of JE, the absence of specific treatments for patients with JE is the crucial factor contributing to poor prognosis [1–3, 5–7]. Therefore, intensive investigation of JEV pathogenic mechanisms is needed for the development of interventional strategies.

Mertk, member of the TAM (Tyro3, Axl and Mertk) family, is a type 1 receptor of tyrosine kinase involved in multiple biological processes by engaging with its bridging ligands Gas6 and Protein S. Gas6 and Protein S bind to phosphatidylserine (PtdSer) displayed on apoptotic cell membranes to initiate subsequent phagocytosis [8]. By taking advantage of this "apoptotic mimicry" form, several enveloped viruses, such as Zika, Ebola, Influenza and SARS-CoV2, incorporate PtdSer into the viral particle membranes to bind Gas6 and Protein S, thus mediating the viral entry and attenuating cellular antiviral response [9–12]. Another distinctive function of TAM-PtdSer pathway is its regulation of innate immunity and inflammation. Deficiencies in TAM receptors have been associated with chronic inflammatory and autoimmune diseases. Enveloped viruses strongly activate TAM receptors to bypass the host immune defense by dampening type I IFN signaling [13]. For example, after infection with vesicular stomatitis virus (VSV), Mertk signaling is activated, IL-10 and TGF-β levels are increased, promoting viral replication [14]. Additionally, TAM and its ligands have been shown to participate in vascular homeostasis by promoting the stabilization of platelet aggregation and survival of endothelial cells. Jonathan et al. found that Mertk could protect against neuroinvasive viral infection by maintaining the integrity of BBB to prevent the virus from invading the central nervous system at early stage, such as West Nile virus (WNV) and La Crosse virus (LACV) [15]. Taken together, accumulating evidence suggests that TAM family exerts diverse functions in viral infectious diseases.

Several studies have shown that systemic immune activation under neurotropic virus infection condition will aggravate the leakage of the BBB, causing the infiltration of numerous virions and activate peripheral immune cells into the brain, leading to an irreversible intracranial inflammatory storm [15–17]. Due to the multifaceted roles of Mertk played in regulation of immunity and vascular permeability, this study intends to uncover the role of Mertk played in JEV pathogenesis.

In this study, we found that Mertk$^{-/-}$ mice exhibited higher mortality and faster disease progression than wild-type mice after JEV infection. This phenotype exhibited by the Mertk$^{-/-}$ mice was mainly associated with enhanced breakdown of the BBB, which could promote viral invasion into the central nervous system and induce more intensive encephalitis.

Materials and methods

Ethical statement

All animal experiments were reviewed and approved by the Animal Care and Use Committee of the Laboratory Animal Center, Air Force Medical University. The number of Animal Experimental Ethical Inspection is 20220109. And all experiments were carried out in accordance with the recommendations set out in the Guide for the Care and Use of Laboratory Animals.

Cells and virus

The JEV-P3 strain was propagated in the brains of 3-day-old inbred BALB/C suckling mice and titrated by conventional plaque assay. The neuroblast cell line Neuro2a, baby hamster kidney (BHK) cells, brain microvascular endothelial cell line bEnd.3, and HEK 293T cells (purchased from American Type Culture Collection (ATCC)) were cultured in Dulbecco's modified Eagle's medium (DMEM, Gibco, United States) containing 10% fetal bovine serum (FBS, Gemini, United States) and 1% penicillin streptomycin combination (Solarbio, China).

Cell culture and JEV infection

Neuro2a cells were seeded in 24 wells with the density of 5×10^3 overnight. The cells were washed by phosphate-buffered saline (PBS) and then infected with JEV (MOI = 1) at 37 °C for 1 h. After adsorption, virus-containing suspension was replaced with fresh DMEM for subsequent cell culture.

Mice

AXL/Mertk double knockout mice were kindly donated by Professor Dai Shu Han (Peking Union Medical College, Chinese Academy of Medical Sciences) and were

maintained in a specific pathogen-free (SPF) facility. AXL/Mertk double knockout mice were backcrossed with wild-type C57BL/6J mice, and toe DNA from newborn mice was extracted and amplified through PCR with PrimeStar (Takara, Japan) for genotyping. Then, the amplified products were analyzed by agarose gel electrophoresis to screen WT, Mertk$^{+/-}$, Mertk$^{-/-}$ descendants (sequences of primers are listed in Supplementary Table S1). The sizes of PCR products are 519 bp for WT mice, 519 and 650 bp for Mertk$^{+/-}$ mice, and 650 bp for Mertk$^{-/-}$ mice.

Mice infection

WT and Mertk$^{-/-}$ mice (6–8 weeks) were inoculated with 1×10^6 plaque-forming units (PFUs) of JEV-P3 in 20 µl of PBS via footpad injection. Body weight, behavior score, and death cases of each group were recorded twice a day at 8:00–9:00 and 16:00–17:00 for 20 days until all the groups were totally stable. The scoring criteria were referred as Bian et al. [18] described. The scoring criteria were as follows: 0: no significant abnormal behaviors, piloerection, restriction of movement, body stiffening, or hind limb paralysis; 1: piloerection, no restriction of movement, body stiffening, or hind limb paralysis; 2: piloerection, restriction of movement, no body stiffening or hind limb paralysis; 3: piloerection, restriction of movement, body stiffening, no hind limb paralysis; 4: piloerection, restriction of movement, body stiffening, and hind limb paralysis; 5: piloerection, restriction of movement, body stiffening, hind limb paralysis, sometimes tremor and even death.

Hematoxylin–eosin (HE) staining

Brain tissues were fixed in 4% paraformaldehyde and embedded in paraffin. Paraffin sections (5 µm) were then dewaxed and hydrated. Subsequently, the sections were sequentially stained with hematoxylin and eosin using a hematoxylin–eosin (HE) staining kit (Servicebio). Finally, the sections were examined under an optical microscope.

Brain sectioning and immunofluorescence staining

Brain tissues used for sectioning and Immunofluorescence staining were obtained from JEV-infected WT and Mertk$^{-/-}$ mice. Mice were subjected to cardiac perfusion under anesthesia, then the brain tissues were collected in 4% PFA. The primary and secondary antibodies used in this study were listed in Supplementary Table S2.

DNA construction

Two shRNA targeting Mertk (sequences in Supplementary Table S3) with the restriction endonucleases AgeI and EcoRI were annealed and inserted into the pLK0.1-puro plasmid. The plasmids from positive clones were extracted and sequenced to obtain the correct recombinant interfering plasmid.

Preparation of recombinant lentiviral particles

Lentiviral pseudoparticles were generated by cotransfecting 293T cells in 6-well plates with the plasmids pLenti-shRNAi-Mertk-puro proviral DNA (3 µg); envelope plasmid (pMD2.G, 1 µg); and packing plasmid (psPAX2, 2 µg). The cell culture medium was changed to 1.7 ml DMEM before transfection. For each transfection, 18 µl transfection regent LipoFectMAX (ABP Biosciences, United States) was mixed with 6 µg total DNA in 0.3 ml DMEM for 30 min and then added to the 6-well plates. The cells were maintained at 37 °C for 6 h, after which the medium was changed with 5 ml DMEM with 10% FBS. The supernatants were harvested at 48 and 72 h. The cell debris was removed by centrifugation at 1000×*g* for 10 min and then 10,000×*g* for 30 min.

Lentivirus infection

bEnd.3 cells were seeded into 6-well plates at 2×10^5 overnight. The supernatant was removed, and 2 ml Mertk-shRNA lentiviral particles mixed with polybrene (8 µg/ml) was added. Lentiviral supernatants were replaced every 2 h until the viral supernatant was used up. Forty eight hours after the infection, fresh DMEM containing puromycin (5 µg/ml) was added to screen the positive cells.

Blood–brain barrier permeability measurements

WT and Mertk$^{-/-}$ mice were injected intraperitoneally with sodium fluorescein solution (0.1 g/ml, 200 µl/mice). After 30 min, eyeball blood was collected into the EP tube pretreated with EDTA-Na2. The peripheral blood cells were removed by cardiac perfusion before brain tissue dissection. The eyeball blood was centrifuged at 6000*g* for 10 min, then 100 µl serum mixed with 100 µl 15% trichloroacetic acid was centrifuged at 10000*g* for 30 min. After weighing the brain tissues, 7.5% trichloroacetic acid was added according to 150 µl/mg and ground with high flux tissue grinder (QIAGEN), then centrifuged at 10000*g* for 30 min. 120 µl centrifugal supernatants obtained from blood and brain tissue respectively were mixed with 30 µl 5M NaOH. 100 µl of the mixture was added to the 96-well blackboard. Fluorescence emission at 485 and 535 nm was determined using multimode microplate reader SPARK (TECAN). The value of fluorescein sodium uptake in the brain tissue was considered as the ratio of brain tissue fluorescence value/plasma fluorescence value.

In vitro BBB model establishment and TEER measurement

The Transwell chamber (Thermo, Waltham, MA, United States) was inverted inserted into 24-well plate, and then C8-Dia cell suspension (25,000/well) was seeded at the bottom side of the chamber and incubated at 37 °C for 6 h. Then Neuro2a cell suspension (5000/well) was inoculated in the 24-well plate, and the chamber was inserted into the corresponding 24-well plate. BEnd.3 or bEnd.3-KD Mertk cell suspension (50,000/well) were then seeded at the upper side of the chamber. The cells were cultured in 10%FBS DMEM medium containing penicillin. Before the daily electrical impedance test, cell culture medium should be replaced with fresh medium. The electrical impedance values were detected by the electrical impedance detector and recorded daily. After about 4 days, the electrical impedance was increased steadily, and a stable liquid column difference was formed compared with the blank chamber, indicating that the in vitro BBB model was successfully constructed. Then the virus was infected and the culture medium was replaced with serum-free DMEM. The virus (MOI = 1) was inoculated onto the Neuro2a cells in the 24-well plate, and the upper chamber was subsequently placed into the 24-well plate for further cultivation. the resistance was detected and recorded every day. The impedance value calculates the TEER = resistance value Ω/0.33 cm.

qRT-PCR

Total RNA from mouse tissues and cells were extracted with Total RNA Kit I (Omega, America). cDNA was prepared by the PrimeScript RT reagent Kit (TaKaRa, Japan). qRT-PCR experiments used SYBR Green Real-Time PCR Master Mix (TaKaRa, Japan) (the primers used were listed in the Supplementary Table S4). The mRNA expression was normalized to β-actin expression, and the data are shown as the relative change to the corresponding reference for each group.

Western blotting

Total protein from the brain of each mouse was extracted with radio-immunoprecipitation assay (RIPA) buffer containing phenylmethanesulfonyl fluoride (PMSF) and phosphatase inhibitors and then quantified by protein reagent assay BCA kit (Thermo, Waltham, MA, United States). Thirty micrograms of protein from each sample were loaded and electrophoresed using sodium dodecyl sulfatepolyacrylamide gel electrophoresis (SDS-PAGE Gel Quick Preparation Kit, Beyotime, China) and transferred protein onto polyvinylidene difluoride (PVDF) membranes (Millipore, Billerica, MA, United States). The membranes were incubated with primary antibodies (antibodies in Supplementary Table S2) overnight at 4 °C, followed by DyLight 800/700-labeled secondary antibodies for 1 h at RT. The blots were visualized using an infrared imaging system (Odyssey, LI-COR, NE, United States).

Plaque assay

BHK cells were cultured overnight in 12-well plates at a density of 2×10^5 per well. The supernatants of the cells were removed, and the cells were washed twice with 1 × PBS solution. Then, the serial 5-fold diluted viral suspension samples with DMEM were added and incubated with BHK cells for 2 h at 37 °C. The viral supernatant was replaced with 4 ml overlay media (25 ml 4 × DMEM, 50 ml 4% methylcellulose, 2 ml FBS, 23 ml ddH2O) and incubated for 5 days. The overlay medium was washed off with 1×PBS several times until the upper overlay was rinsed, and then cells in each well were immobilized with 2 ml Crystal violet dye for 15 min. Finally, 12-well plate was washed with flowing tap water and plaques were counted.

Enzyme-linked immunosorbent assay

The enzyme-linked immunosorbent assay (ELISA) kit (Proteintech, China) was used to detect the concentration of inflammatory cytokines in serum of WT and Mertk$^{-/-}$ mice, such as tumor necrosis factor-α (TNF-α), interleukin-10 (IL-10) and IL-6. Twenty-five microliters of serum were added to the enzyme-labeled plate coated with TNF-α antibody, and incubated at 37 °C for 2 h. Then, the serum was removed, the plate was washed with wash buffer for four times, and TNF-α antibody was added for another 60 min. Subsequently, the working solution of the enzyme conjugate was added to the plate, and the plate was incubated for 40 min. After washing the plate, the color-developing substrate was added, and the plate was incubated for 15 min. The optical density (OD) at 450 nm was measured using a microplate reader after the termination liquid was added. The contents of IL-10 and IL-6 were detected using the same procedure as that for TNF-α.

Statistical analysis

All statistical analysis were performed using GraphPad Prism version 8 software. Statistical differences were determined using Student's t-test or two-way analysis of variance (ANOVA). P-values < 0.05 were considered significant.

Results

Mertk knockout mice are highly susceptible to JEV infection

To determine the role of Mertk in the pathogenesis of JEV infection, we evaluated the survival rate, body weight and neurobehavioral score of both WT and Mertk$^{-/-}$ mice

group after JEV infection. The mortality of wild-type mice inoculated with JEV at 10^6 PFU was about 60%, while that of Mertk$^{-/-}$ mice was 100% (Fig 1A). The median survival time of infected Mertk$^{-/-}$ mice was also shorter than WT group. In addition, JEVchallenged Mertk$^{-/-}$ mice exhibited higher behavioral scores and faster weight loss compared to WT mice (Fig 1B, C). The high morbidity and mortality observed in JEV-infected Mertk$^{-/-}$ mice suggest a protective role of Mertk during JEV infection.

No significant difference in viral replication and inflammatory cytokines in the peripheral tissue of JEV-infected WT and Mertk$^{-/-}$ mice

Since the pathophysiology caused by viral infection in peripheral tissues are closely related to brain tissue for viral encephalitis, we next had detected the viral load and expression levels of immune response-related cytokines in the peripheral tissues of JEV-infected WT and Mertk$^{-/-}$ mice at different time-points. The JEV replication kinetics in the serum of WT and Mertk$^{-/-}$ mice measured by plaque assay demonstrated similar viremia at different time points after JEV infection (Fig. 2A). We next detected the JEV RNA copies in the spleens of WT and Mertk$^{-/-}$ mice infected with JEV. Nonetheless, there was no significant difference in JEV RNA levels in the spleens of WT and Mertk$^{-/-}$ mice after infection (Fig. 2B). These data suggested that Mertk had no significant effect on peripheral viral load restriction during JEV infection.

Recent works have implicated that the TAM pathway could alleviate immunopathological injury by negatively regulating the inflammatory response. It is known that JEV infection can induce a strong up-regulation of multiple inflammatory cytokines and chemokines, which in turn mediate the severe immunopathological damage. Therefore, we next assessed the expression levels of classical inflammatory cytokines in the spleen by qPCR. Although the expression levels of IL-1β and TNF-α were higher in Mertk$^{-/-}$ mice than WT mice at day 5 post of infection (Fig. 2C–G), overall, the expression levels of other inflammatory cytokines induced by JEV infection were comparable in the spleen of WT and Mertk$^{-/-}$ mice. Furthermore, the expression of inflammatory cytokines in serum of WT and Mertk$^{-/-}$ mice on the 3rd day of infection was determined by ELISA (Fig. 2H–J). The results showed that there was no significant difference in the expression of IL-10, IL-6 and TNF-α in serum of WT and Mertk$^{-/-}$ mice. Collectively, our data suggested that the protective effect of Mertk against JEV infection is independent of its function in the periphery.

Significantly increased viral load in the brain tissues from Mertk$^{-/-}$ mice after JEV infection

Since Mertk had no significant effect on viral replication and inflammatory response in the periphery, we further intended to investigate the role of Mertk in the central nervous system (CNS). Therefore, we detected the JEV mRNA level and viral protein expression level in the brain tissues from WT and Mertk$^{-/-}$ mice infected subcutaneously with JEV. The results showed that both the viral mRNA level (Fig. 3A) and the viral non-structural protein NS3 expression level (Fig. 3B) were significantly higher in the brain tissues of Mertk$^{-/-}$ mice compared with WT mice at 5 days post of JEV infection.

Meanwhile, we examined the mRNA levels of several inflammatory cytokines in the brain tissues of Mertk$^{-/-}$ and WT mice. The results showed that the inflammatory

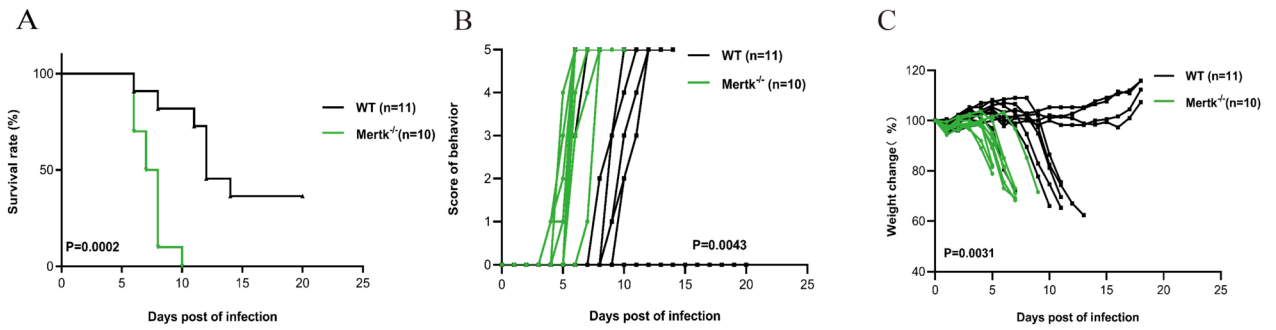

	WT (n=11)	Mertk$^{-/-}$ (n=10)
Median survival	12	7.5
Mortality rates	60%	100%

Fig. 1 Mertk KO mice are highly susceptible to JEV infection. WT (n = 11) and Mertk$^{-/-}$ (n = 10) mice were administered with JEV P3 strain (1×10^6 PFU) in-footpad per mouse. Survival (**A**), behavior score (**B**) and body weight changes (**C**) of WT and Mertk$^{-/-}$ mice were monitored for 20 days after JEV challenge

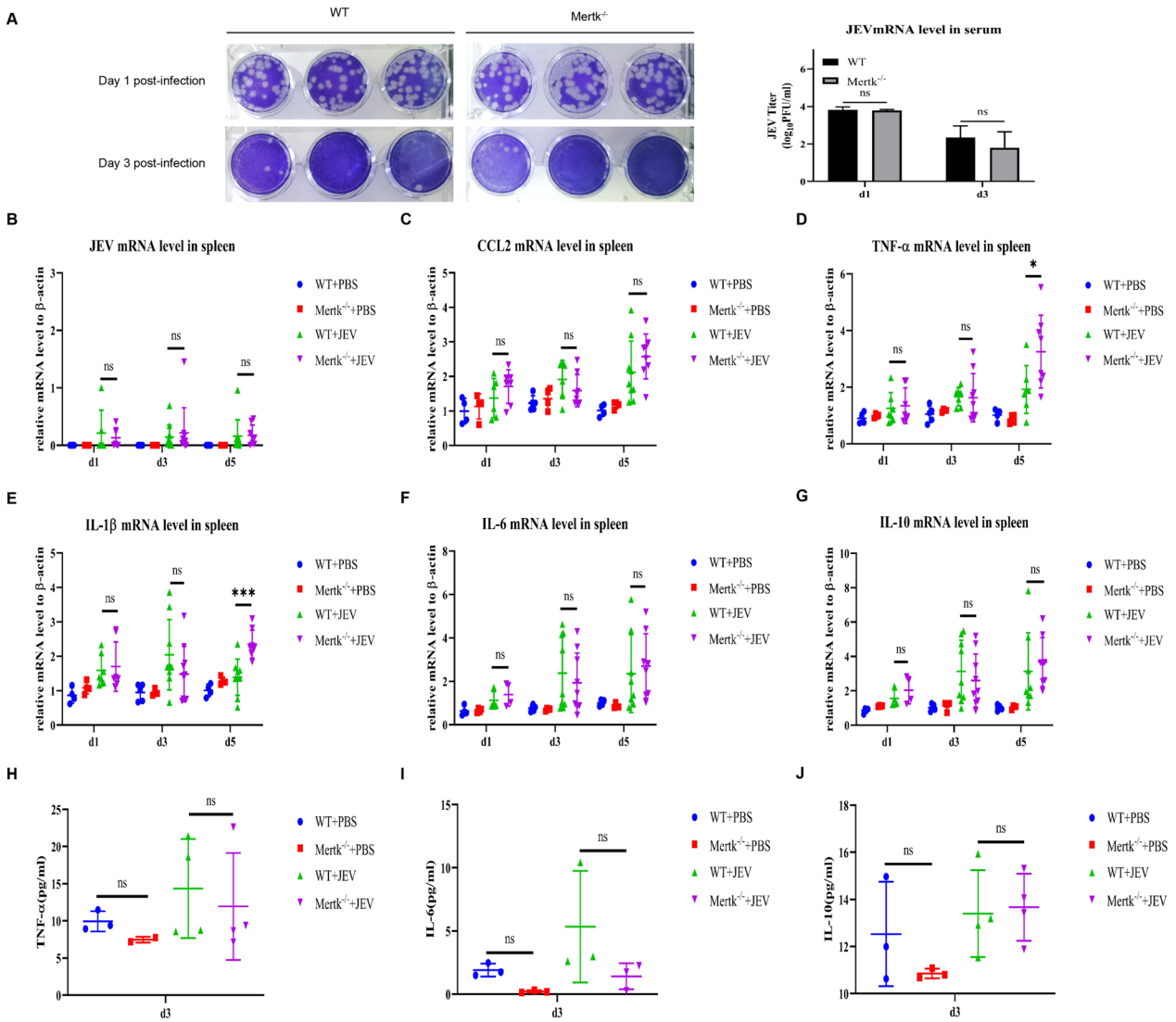

Fig. 2 Viral load and inflammatory response in peripheral were not significantly changed between WT and Mertk$^{-/-}$ mice after JEV infection. **A** Blood sample were collected from mice tail vein at 1 day and 3 days after JEV infection in WT (n = 3) and Mertk$^{-/-}$ (n = 3) mice. Plague formation assay was performed to determinate virus titers in peripheral. **B**–**G** Profiles of JEV mRNA level (**B**) and inflammatory genes (**C**–**G**) in spleen of WT and Mertk$^{-/-}$ mice were detected at 1 day (WT + PBS n = 4, Mertk$^{-/-}$ + PBS n = 4, WT + JEV n = 7, Mertk$^{-/-}$ + JEV n = 7), 3 days (WT + PBS n = 5, Mertk$^{-/-}$ + PBS n = 4,WT + JEV n = 12, Mertk$^{-/-}$ + JEV n = 11) and 5 days (WT + PBS n = 4, Mertk$^{-/-}$ + PBS n = 4,WT + JEV n = 11, Mertk$^{-/-}$ + JEV n = 11) after JEV infection by qPCR. The expression level was normalized to WT mice treated with PBS. **H**–**J** Levels of the proinflammatory cytokines interleukin (IL)-10, IL-6, and tumor necrosis factor alpha (TNF-α) in the serum of WT and Mertk$^{-/-}$ mice were detected by enzyme-linked immunosorbent assay (WT + PBS n = 3, Mertk$^{-/-}$ + PBS n = 3, WT + JEV n = 4, Mertk$^{-/-}$ + JEV n = 4). *$P < 0.05$, **$P < 0.01$ and ***$P < 0.001$

cytokines, including TNF- α, IL-1 β, IL-6 and IL-10, were at comparable levels, except that the level of CCL2 was significantly increased in Mertk$^{-/-}$ mice (Fig. 3A).

Further histopathological evaluation also confirmed that there was no significant difference in necrosis, astrocytosis and hemorrhage in the brain tissues between WT and Mertk$^{-/-}$ mice after JEV infection (Fig. 3C). These data suggested that the absence of Mertk caused an increased viral load in the CNS, but had little effect on the inflammatory response and immunopathological damage in the brain.

Mertk is critical for maintaining the integrity of blood–brain barrier

Since Mertk knockout had resulted in increased CNS viral load, but no significant changes were observed in peripheral or central immune response, we hypothesized that increased viral invasion might be responsible for the

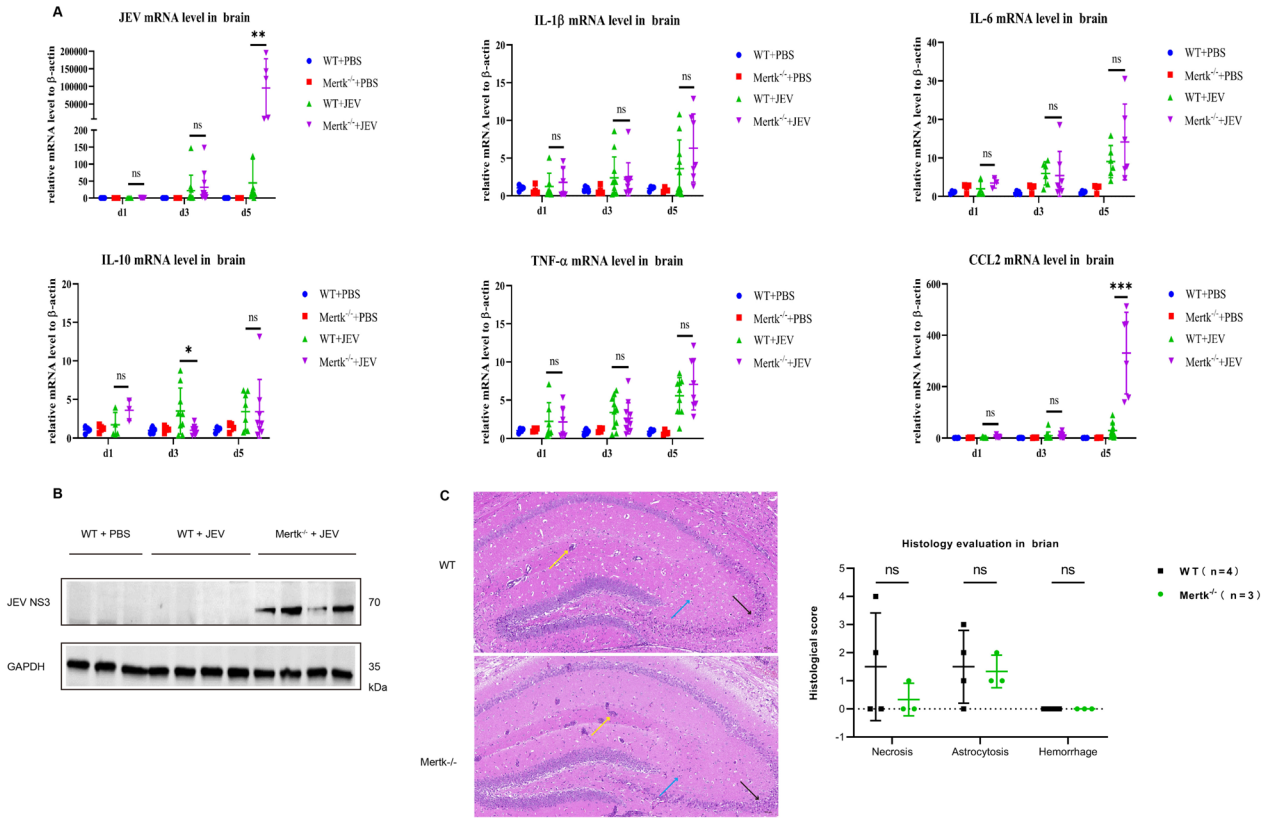

Fig. 3 JEV titer in brain was increased in Mertk$^{-/-}$mice. **A** JEV mRNA level and inflammatory genes profiles in brain of WT and Mertk$^{-/-}$ mice were detected at 1 day(WT + PBS n = 4, Mertk$^{-/-}$ + PBS n = 4, WT + JEV n = 7, Mertk$^{-/-}$ + JEV n = 7), 3 days (WT + PBS n = 5, Mertk$^{-/-}$ + PBS n = 4,WT + JEV n = 12, Mertk$^{-/-}$ + JEV n = 11) and 5 days (WT + PBS n = 4, Mertk$^{-/-}$ + PBS n = 4,WT + JEV n = 11, Mertk$^{-/-}$ + JEV n = 11) after JEV infection by qPCR. The expression level was normalized to WT mice treated with PBS. **B** JEV NS3 and β-actin expression levels in PBS or JEV treated WT and Mertk$^{-/-}$ mice were detected by western blot at 5 days after JEV infection (PBS-treated WT n = 3, JEV-treated WT n = 4, JEV-treated Mertk$^{-/-}$ n = 4). **C** Representative histology of mice brain analyzed by HE staining and the histology evaluation of necrosis, astrocytosis and hemorrhage. (Yellow arrow: intravascular leucocyte, blue arrow: astrocytosis, black arrow: abundant eosinophilic granular cytoplasm) *$P < 0.05$, **$P < 0.01$ and ***$P < 0.001$

accumulation of virus in the brain. It is known that BBB is an important barrier preventing pathogens from invading the CNS. And previous studies have identified Mertk as a critical maintainer of BBB integrity [15]. As a result, we found that in Mertk knockout mice, JEV virus replication in brain was more obvious. To detect whether the disruption of BBB integrity induced by the knockout of Mertk is a possible factor contributing to the excessive leakage of the viral particles into the brain, We examined the integrity of BBB in JEV-infected Mertk$^{-/-}$ mice and WT mice. At the 4 days after JEV infection, we found that the leakage of fluorescent dye NaF was significantly higher in the brain of Mertk$^{-/-}$ mice than in the WT group, suggesting that Mertk$^{-/-}$ mice exhibited higher BBB permeability and lower BBB integrity (Fig. 4A).

To explore whether Mertk modulates BBB integrity and JEV invasion, we constructed an in vitro model of BBB with endothelial cell line bEnd.3 with or without Mertk knock down (Fig. 4B). By measuring the electrical impedance of the in vitro BBB model(Fig. 4C), we found that the electrical resistance in the BBB model constructed with bEnd.3-KD Mertk cells were significantly lower than that in bEnd.3 cells at 24 and 48 h after JEV infection (Fig. 4D).

Tight junction proteins in the brain are important to establish and maintain the integ rity of BBB [19]. Since knockdown of Mertk in endothelial cell line increased the permeability of the in vitro BBB model, we further detected the distribution and expression of CD31 (classical marker of vascular endothelial cells) and ZO-1 (tight junction protein) in the brain tissues in PBS-treated and JEV-infected Mertk$^{-/-}$ mice and WT mice (Fig. 4E, F). Immunofluorescence results showed that the integrity and continuity of ZO-1 and CD31 in the brain of Mertk$^{-/-}$ mice were decreased compared to WT mice at day 5 post of JEV infection. These data indicated that Mertk maintains BBB integrity both in vitro and in vivo to prevent the peripheral virus from invading the CNS.

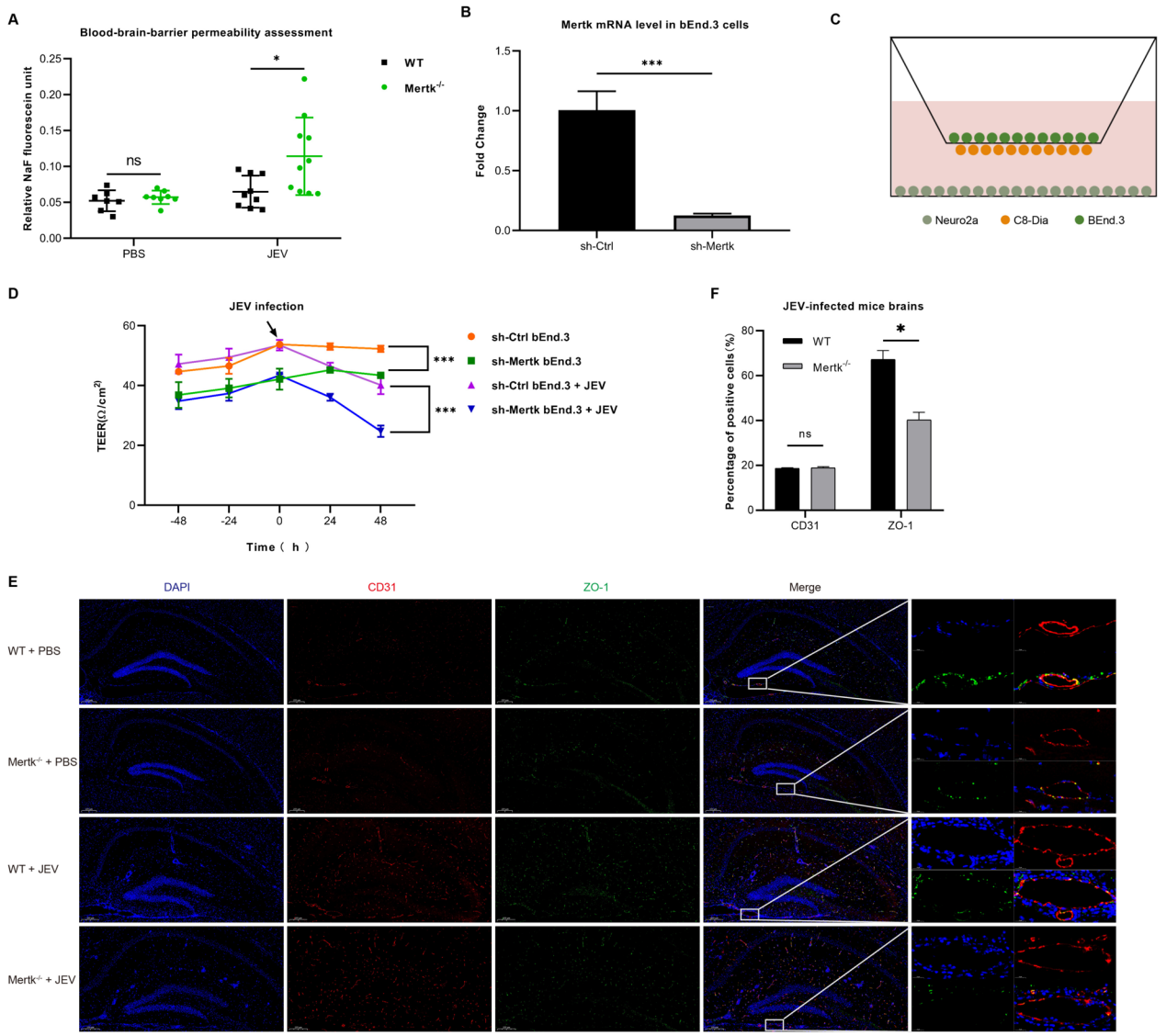

Fig. 4 Mertk knockout mice exhibited impaired blood–brain-barrier integrity under JEV challenging condition. **A** BBB permeability was measured in terms of NaF accumulation in brain of WT and Mertk$^{-/-}$ mice at 4 days (PBS-treated WT n = 7, PBS-treated Mertk$^{-/-}$ n = 8, JEV-treated WT n = 11, JEV-treated Mertk$^{-/-}$ n = 11) after JEV infection. **B** Knockdown of Mertk in BEnd.3 cell line using lentiviral expression system were in identified by qPCR. **C** Graphical representation of in vitro BBB model. **D** Normalized TEER values of BBB model were monitored per day to reveal BBB integrity. **E** Immunofluorescence analysis of CD31 and ZO-1 expression in mice brain at 5 days after PBS or JEV infected WT and Mertk$^{-/-}$ mice. Endothelium stained by CD31 antibody is displayed in red, ZO-1 is displayed in green, the nucleus stained with DAPI is shown in blue. Scale bar: 20 μm. **F** Quantitative analysis of CD31 and ZO-1 expression in WT and Mertk$^{-/-}$ mice infected with JEV. *$P < 0.05$, **$P < 0.01$ and ***$P < 0.001$

Discussion

Mertk is a tyrosine kinase receptor involved in pathogen entry, phagocytosis of apoptotic cells, inflammatory response regulation and the maintenance of BBB. In this study, we found that Mertk deficient mice exhibited higher mortality and faster disease progression than wild-type mice after JEV infection. Mertk deficiency did not directly affect viral replication and immune response in peripheral, but caused increased viral load in the CNS, which was correlated with the enhanced BBB penetration. Our data suggested that Mertk acts as a protective factor in the development of encephalitis induced by JEV infection, which is mainly associated with its beneficial effect on BBB integrity to inhibit the entry of peripheral JEV into CNS, rather than its regulation of inflammatory response.

Previous reports showed that Axl, another member of the TAM family, can mediate the entry of DENV

and ZIKV into host cells by usurping the apoptotic cell clearance pathway (bridging viral membrane PtdSer with Gas6 and Protein S) [20, 21]. In the context of JEV infection, Axl could impede the pathogenesis of severe JE in mice by maintaining BBB integrity and restricting viral neural invasion [15, 22]. These observations prompted us to investigate the role of Mertk in encephalitis induced by JEV infection. Here we found that JEV-infected Mertk$^{-/-}$ mice exhibited increased morbidity and mortality and faster weight loss compared to WT mice, suggesting that Mertk may play a protective role in the development of encephalitis.

It is known that TAM family exert a negative regulatory effect on innate immune response to microbial infection [23–25]. In the present study, we observed no discernible differences in either viral titers or inflammatory cytokines expression levels in the peripheral tissues of Mertk$^{-/-}$ mice compared to WT mice after footpad inoculation with JEV.

Extensive replication of JEV within the CNS and severe immunopathological damage caused by intracranial immune activation are key events in the progression of JEV-induced encephalitis [4, 7]. Therefore, we further investigated the function of Mertk in the CNS. Our data showed that viral load was significantly elevated in the brain tissues of Mertk$^{-/-}$ mice compared to WT mice, suggesting that Mertk deficiency caused an increased viral load in the CNS, however, had no significant effect on the inflammatory response and immunopathological damage in the brain. Surprisingly, the level of CCL2 in the brain was significantly increased in Mertk$^{-/-}$ mice compared with WT mice. Several reports showed that neurons are a key source of CCL2 during the earliest stages of neurotropic virus infection [26, 27]. The mechanism by which CCL2 upregulation in Mertk$^{-/-}$ mice infected with JEV is currently being studied.

Several studies found that knockdown or blockade of TAM can reduce the integrity of the BBB and promote neurotropic virus invasion into the CNS [15]. Therefore, we further examined the integrity of BBB to determine whether the deficiency of Mertk was associated with the leakage of BBB, thus causing the intracranial accumulation of JEV. Through sodium fluorescein penetration test and tissue immunofluorescence analysis, we found that the BBB permeability of Mertk$^{-/-}$ mice was significantly higher than that of WT mice after JEV infection, along with the decreased integrity and continuity of ZO-1 and CD31 in brain tissues of Mertk$^{-/-}$ mice. Moreover, we constructed an in vitro BBB model and further determined that downregulation of Mertk in endothelial cells also increased the permeability of BBB. These results indicated that Mertk is a vital factor in maintaining BBB integrity, thus preventing virus dissemination to the brain.

Our study has uncovered the potential protective role of Mertk in mice infected with JEV for the first time. However, further research are needed to investigate the specific molecular regulatory mechanism of Mertk in maintaining BBB integrity and preventing JEV invasion into the CNS.

Supplementary Information

The online version contains supplementary material available at https://doi.org/10.1186/s12985-024-02472-1.

Supplement Figure 1: Phenotype verification of Mertk KO mice. Tissue DNA were extracted from mice tail and PCR was used to identify wild-typeand Mertk KOgenotypes

Additional file2

Additional file3

Author contributions

Conceptualization, L-Y.F.; methodology, L-C.Y., B-P.Y. and L-Y.F.; software, Y-C.T. and D-Y.C.; validation, L-C.Y. and L-X.M.; formal analysis, L-C.Y., L-M.Y., B-P.Y. and Y-J.L.; investigation, L-C.Y., B-P.Y. and Y-J.L.; resources, L-Y.F. and Z-Q.Q.; data curation, L-C.Y. and L-M.Y.; writing—original draft preparation, L-C.Y. and L-M.Y.; writing—review and editing, L-C.Y.,L-M.Y. and L-Y.F.; visualization, L-C.Y.,L-M.Y. and L-Y.F.; supervision, L-Y.F., Z-Q.Q. and Z-F.L.; project administration, L-Y.F., Z-Q.Q. and L.X.; funding acquisition, L-Y.F. All authors have read and agreed to the published version of the manuscript.

Funding

This research was funded by the National Natural Science Foundation of China, Grant No. 81871697.

Data availability

No datasets were generated or analysed during the current study.

Declarations

Human or animal rights

The animal study involved in our study was reviewed and approved by the Animal Care and Use Committee of the Laboratory Animal Center, Air Force Medical University. The number was provided in the Human and animal rights section.

Competing interests

The authors declare no competing interests.

Received: 5 March 2024 Accepted: 14 August 2024
Published online: 14 September 2024

References

1. Schuh AJ, Ward MJ, Leigh BAJ, et al. Dynamics of the emergence and establishment of a newly dominant genotype of Japanese encephalitis virus throughout Asia. J Virol. 2014;88(8):4522–32.
2. Diallo AOI, Chevalier V, Cappelle J, et al. How much does direct transmission between pigs contribute to Japanese encephalitis virus circulation? A modelling approach in Cambodia. PLoS ONE. 2018;13(8):e0201209.
3. Samy AM, Alkishe AA, Thomas SM, et al. Mapping the potential distributions of etiological agent, vectors, and reservoirs of Japanese encephalitis in Asia and Australia. Acta Trop. 2018;188:108–17.

4. Hsieh JT, St. John AL. Japanese encephalitis virus and its mechanisms of neuroinvasion. PLoS Pathog. 2020;16(4):e1008260.
5. Wang H, Liang G. Epidemiology of Japanese encephalitis: past, present, and future prospects. Ther Clin Risk Manag. 2015;11:435–48.
6. Banerjee A, Tripathi A. Recent advances in understanding Japanese encephalitis. F1000Res. 2019;8(F1000 Faculty Rev):1915. https://doi.org/10.12688/f1000research.19693.1.
7. Joe S, Salam AAA, Neogi U, et al. Antiviral drug research for Japanese encephalitis: an updated review. Pharmacol Rep. 2022;74(2):273–96.
8. Geng K, Kumar S, Kimani SG, et al. Requirement of gamma-carboxyglutamic acid modification and phosphatidylserine binding for the activation of Tyro3, Axl, and Mertk receptors by growth arrest-specific 6. Front Immunol. 2017;8:1521.
9. Vernon PJ, Tang D. Eat-me: autophagy, phagocytosis, and reactive oxygen species signaling. Antioxid Redox Signal. 2013;18(6):677–91.
10. Graham DK, Deryckere D, Davies KD, et al. The TAM family: phosphatidylserine sensing receptor tyrosine kinases gone awry in cancer. Nat Rev Cancer. 2014;14(12):769–85.
11. Zheng G, Li LF, Zhang Y, et al. MERTK is a host factor that promotes classical swine fever virus entry and antagonizes innate immune response in PK-15 cells. Emerg Microbes Infect. 2020;9(1):571–81.
12. Wang ZY, Wang PG, An J. The multifaceted roles of TAM receptors during viral infection. Virol Sin. 2021;36(1):1–12.
13. Rothlin CV, Carrera-Silva EA, Bosurgi L, et al. TAM receptor signaling in immune homeostasis. Annu Rev Immunol. 2015;33:355–91.
14. Adomati T, Cham LB, Hamdan TA, et al. Dead cells induce innate anergy via mertk after acute viral infection. Cell Rep. 2020;30(11):3671-81.e5.
15. Miner JJ, Daniels BP, Shrestha B, et al. The TAM receptor Mertk protects against neuroinvasive viral infection by maintaining blood–brain barrier integrity. Nat Med. 2015;21(12):1464–72.
16. Komarasamy TV, Adnan NAA, James W, et al. Zika virus neuropathogenesis: the different brain cells, host factors and mechanisms involved. Front Immunol. 2022;13:773191.
17. Trivedi S, Chakravarty A. Neurological complications of dengue fever. Curr Neurol Neurosci Rep. 2022;22(8):515–29.
18. Bian P, Ye C, Zheng X, et al. RIPK3 promotes JEV replication in neurons via downregulation of IFI44L. Front Microbiol. 2020;11:368.
19. Castaneda-Cabral JL, Colunga-Duran A, Urena-Guerrero ME, et al. Expression of VEGF- and tight junction-related proteins in the neocortical microvasculature of patients with drug-resistant temporal lobe epilepsy. Microvasc Res. 2020;132:104059.
20. Meertens L, Carnec X, Lecoin MP, et al. The TIM and TAM families of phosphatidylserine receptors mediate dengue virus entry. Cell Host Microbe. 2012;12(4):544–57.
21. Strange DP, Jiyarom B, Pourhabibi ZN, et al. Axl promotes zika virus entry and modulates the antiviral state of human sertoli cells. MBio. 2019;10(4):e01372–19.
22. Wang ZY, Zhen ZD, Fan DY, et al. Axl deficiency promotes the neuroinvasion of Japanese encephalitis virus by enhancing IL-1alpha production from pyroptotic macrophages. J Virol. 2020;94(17):e00602–20.
23. Li Q, Lu Q, Lu H, et al. Systemic autoimmunity in TAM triple knockout mice causes inflammatory brain damage and cell death. PLoS ONE. 2013;8(6):e64812.
24. Meertens L, Labeau A, Dejarnac O, et al. Axl mediates ZIKA virus entry in human glial cells and modulates innate immune responses. Cell Rep. 2017;18(2):324–33.
25. Chen J, Yang YF, Yang Y, et al. AXL promotes Zika virus infection in astrocytes by antagonizing type I interferon signalling. Nat Microbiol. 2018;3(3):302–9.
26. Howe CL, Lafrance-Corey RG, Goddery EN, et al. Neuronal CCL2 expression drives inflammatory monocyte infiltration into the brain during acute virus infection. J Neuroinflamm. 2017;14(1):238.
27. Vidana B, Johnson N, Fooks AR, et al. West Nile virus spread and differential chemokine response in the central nervous system of mice: role in pathogenic mechanisms of encephalitis. Transbound Emerg Dis. 2020;67(2):799–810.

Publisher's Note